



**ARTICLE**

## Flow and Melting Thermal Transfer Enhancement Analysis of Alumina, Titanium Oxide-Based Maxwell Nanofluid Flow Inside Double Rotating Disks with Finite-Element Simulation

Liangliang Chen<sup>1</sup>, Madeeha Tahir<sup>2,\*</sup>, Sumeira Yasmin<sup>3</sup>, Taseer Muhammad<sup>4</sup>, Muhammad Imran<sup>5,\*</sup> and Fenghua Liu<sup>1</sup>

<sup>1</sup>Chongqing Water Resources and Electric Engineering Collage, Chongqing, 402160, China

<sup>2</sup>Department of Mathematics, Government College Women University, Faisalabad, 38000, Pakistan

<sup>3</sup>Department of Mathematics, Government College University Faisalabad, Layyah Campus, Layyah, 31200, Pakistan

<sup>4</sup>Department of Mathematics, College of Sciences, King Khalid University, Abha, 61413, Saudi Arabia

<sup>5</sup>Department of Mathematics, Government College University, Faisalabad, 38000, Pakistan

\*Corresponding Authors: Madeeha Tahir. Email: dr.madeeha.2017@gmail.com; Muhammad Imran  
Email: drminranranchaudhry@gmail.com

Received: 19 May 2021 Accepted: 17 September 2021

### ABSTRACT

The energy produced by the melting stretching disks surface has a wide range of commercial applications, including semi-conductor material preparation, magma solidification, permafrost melting, and frozen land refreezing, among others. In view of this, in the current communication we analyzed magnetohydrodynamic flow of Maxwell nanofluid between two parallel rotating disks. Nanofluids are important due to their astonishing properties in heat conduction flows and in the enhancement of electronic and manufacturing devices. Furthermore, the distinct tiny-sized particles  $Al_2O_3$  and  $TiO_2$  in the Maxwell water-based fluid for enhancing the heat transfer rate are analyzed. The heat equation is developed in the occurrence of thermal radiation. The influences of melting impacts are incorporated. The mathematical model is developed in the form of partial differential expressions then converted to ordinary differential equations by employing tool of similarity variables. Finite element method (FEM) is chosen for solving the nonlinear governing ordinary differential equations (ODEs) with necessary conditions. The consequence of flow parameters against the velocity profiles and heat transport field is considered. The noted novelty of this communication is to discuss the thermal transfer of Maxwell nanofluid model through double stretching disks with thermal radiation and melting phenomenon. Further,  $Al_2O_3$ /water and  $TiO_2$ /water are considered in the modeling.

### KEYWORDS

Maxwell nanofluid; melting phenomenon; thermal radiation; revolving stretching disks; finite element method (FEM)



**Nomenclature**

$\beta_0$	Magnetic field strength
$Nu_x$	Nusselt number
$P$	Pressure
$\theta$	Dimensionless temperature
$B_2$	Stretching parameter at upper disk
$Pr$	Prandtl number
$T_1$	Ambient temperature attained
$q_r$	Radiative heat flux
$T$	Fluid temperature
$Rd$	Radiation parameter
$C_f$	Skin friction coefficient
$Re$	Reynolds number
$\rho_f$	Base fluid density
$\rho_p$	Nanoparticle mass density
$f(\zeta)$	dimensionless stream function
$(\rho c_p)_{nf}$	Nanofluid heat capacitance
$g$	Gravitational acceleration
$\rho_{nf}$	Nanofluid density
$\mu$	Viscosity of fluid
$\psi$	Stream function
$K^*$	Coefficient of mean absorption
$a$	Constant
$\sigma$	Electric conductivity
$\sigma^*$	Stephan-Boltzmann constant
$k_s$	Thermal conductivity of nanoparticles
$\varepsilon$	Pressure parameter
$M$	Magnetic parameter
$\tau_w$	Shear stress
$\alpha$	Thermal diffusivity of base fluid
$\beta$	Maxwell parameter
$\zeta$	Similarity variable
$\omega_1, \omega_2$	Angular velocities
$k_{nf}$	Nanofluid thermal conductivity
$b_1, b_2$	Different stretching rates

**1 Introduction**

Advanced technologies realize the critical value of a unique type of energy transport fluids known as nanoliquid, because of the growing requirements of heat. The most significant aspect of the heat transfer system is the heat efficiency of the base fluid. Since non-metallic materials have poorer thermal efficiency than metallic substances. High thermal efficiency nanoparticles dispersed in regular fluids, which are typically made up of metals and oxides, greatly improve the heat proficiency of the host liquid. Therefore, metals are more useful to improving the thermal transfer rate. Choi and Eastman in (1995) coined the term “nanofluid” to describe the regular fluid that contained very tiny (1–100 nm) nanomaterials. Hayat et al. [1] reviewed the analysis of activation in Ree-Eyring nanofluid flow inside double disks. Qayyum et al. [2] scrutinized the entropy production inspirations on Williamson nanoliquid flow insides double rotating disks. Muhammad et al. [3] observed the slip impacts with activation energy across a three-dimensional sheet. Rafiq et al. [4] examined the numerical computations effects of nanofluid containing

six different particles namely *Ag*, *Cu*, *CuO*, *Fe<sub>3</sub>O<sub>4</sub>*, *TiO<sub>2</sub>* and *Al<sub>2</sub>O<sub>3</sub>*. Hassan et al. [5] debated *Cu–Ag/water* hybrid nanofluid flow through a cone. Sheikholeslami et al. [6] illustrate the impact of electro-hydrodynamic flow of *Fe<sub>3</sub>O<sub>4</sub>*–ethylene glycol nanofluid over an enclosure. The effects of magnetic fields on the hybrid nanomaterials are scrutinized by Shah et al. [7]. Arefmanesh et al. [8] discussed the influence of mixed convection in nanofluid through wavy wall cavity. Ashraf et al. [9] introduced the thermal transfer improvement in blood-base nanofluid across wavy tube. The theoretical analysis of three-dimensional Newtonian nanofluids with permeability porous medium is also examined by Ullah et al. [10]. Lu et al. [11] examined the squeezing flow of nanoliquid by adopting MDP.

The development of hybrid nanofluids, which are essentially an aqueous mixture of two or more forms of nanostructures in mixture or composite shape, is the next advancement in nanofluids technology. Hybrid nanofluids are being developed to solve the drawbacks of single suspension and to take benefit of nanoparticle synergy. Hybrid nanomaterials demonstrated that nanofluids have enhanced energy transfer and thermal conductivity, resulting in cost savings in commercial applications. There is little experimental, theoretical, and computational research on hybrid nanofluids. Li et al. [12] simulated the fractional study of hybrid nanoliquid flow across a spinning disk. Gul et al. [13] highlights the conical gap between cone and disk under hybrid nanofluid flow by adopting Homotopy analysis method. Waqas et al. [14] introduced the hybrid nanofluid flow over radiative disk. Shafee et al. [15] introduced the Entropy generation effects along NEPCM charging mechanics utilizing hybrid nanomaterials. Armaghani et al. [16] discussed the role of magnetized hybrid nanofluid flow through L-shape cavity. Shoaib et al. [17] explored the joule heating effects on magneto hybrid nanofluid over radiative rotating disk. The significance of magnetic dipole in hybrid nanofluid across stretchable surface is illustrated by Gul et al. [18]. Several evaluations have been discussed and presented in the literature, see for illustration [19,20].

Magnetohydrodynamics (MHD) is a class of physics that describes the magnetic properties of electrically interacting liquids. It usually influences thermal transport and manifests itself as Joule heating and Lorentz strength. MHD includes things like refrigerator cooling, saltwater, plasma, tumor therapy, X-ray radiation, and electrolytes. Many excellent works describing various aspects of MHD have been released. Reddy et al. [21] explored the MHD *Cu – Ag/water* mono nanoliquid flow. The significant features of flow and thermal transfer in *Cu/water* nanofluid inside double plates are scrutinized by Wakif et al. [22]. The effects of entropy generation on magnetized hybrid nanoliquid flowing configured by a sheet are investigated by Mumraiz et al. [23].

The concept of porous media is used in various fields of technology and applied science, including mechanics, filtration, petroleum engineering, construction engineering, hydrogeology, and biophysics. MHD *CuO – water* nanofluid flow within the porous cavity was explored by Sheikholeslami [24]. Waqas et al. [25] analyzed the viscous nanofluid flowing across a porous stretchable revolving disk embedded in porous medium. The features of second order slip on nanofluid contain nano-sized nanomaterials past curved channels under porous permeability are explored by Riaz et al. [26].

The thermal radiation behavior in thermal transfer has applications in a variety of thermal engineering fields, including hybrid power solar systems, rocket propulsion, nuclear reactors, rockets, aircraft, and communication technology. It is worth noting that linear radiation is adequate to produce thermal equipment and is widely used in several technological processes. Hayat et al. [27] analyzed the impacts of thermal radiation on *Carbon/water* nanofluid. The behavior of thermal radiation in hydrothermal nature of nanofluid is scrutinized by Sheikholeslami et al. [28]. Li et al. [29] numerically investigate the radiative modified second grade nanofluid aspects. Naqvi et al. [30] studied the heat radiation effects on Casson nanofluid in the occurrence of magnetic field.

Melting heat has piqued the interest of scientists and researchers owing to its various uses in novel industrial processes. In recent times, scientists have concentrated their efforts on creating more long-term, reliable, and affordable energy storing technologies. Unintended thermal efficiency, solar energy and power are all examples of such technologies. Roberts [31] the first to depict the nature of melting thermal transfer in a hot air stream of ice surface. The behavior of melting impact with bioconvection in generalized second grade nanofluid configured by stretching surface is illustrated by Waqas et al. [32]. Hayat et al. [33] introduced the melting thermal transport in stagnation point flow of nanofluid with zero mass flux condition across a stretching surface. Ullah et al. [34] discussed the numerical solution of *SWCNTs – MWCNTs/Engine oil* hybrid nanofluid flow with melting mechanism. The behavior of melting heat on magneto nanofluid flow past stretching sheet is analyzed by Sharma et al. [35].

As reviewed above, the non-Newtonian nature of nanofluid has vital applications. The key determination of this article is to scrutinize the MHD flow and melting heat transfer for a nanofluid model through a two parallel rotating disks. Novelty of the communication is firstly to scrutinize the axisymmetric flow of Maxwell-water based nanofluid with thermal radiation. Secondly the numerical solution of current problem is solved numerically by applied Finite element method. The numerical solutions are obtained and the role of physical factors on the subjective dimensionless profiles is scrutinized and reflected by graphs.

## 2 Mathematical Modeling

### 2.1 Mathematical and Physical Flow Description

Considerable the effect of steady incompressible, axisymmetric electromagnetic flow with heat transformation by using different particles based on Maxwell nanofluid between both revolving stretching disks at the distance  $h$  from upper to lower disks. The upper and lower disks have the distinct angular velocities denoted by  $(\omega_1 \& \omega_2)$  and both disks have distinct stretching rates  $(b_1 \& b_2)$  along the radial direction and axial direction correspondingly. The magnetic field strength  $B_0$  along  $z$  – axis is presented and the cylindrical coordinate system  $(r-, \theta-, z-)$  is considered in Fig. 1.

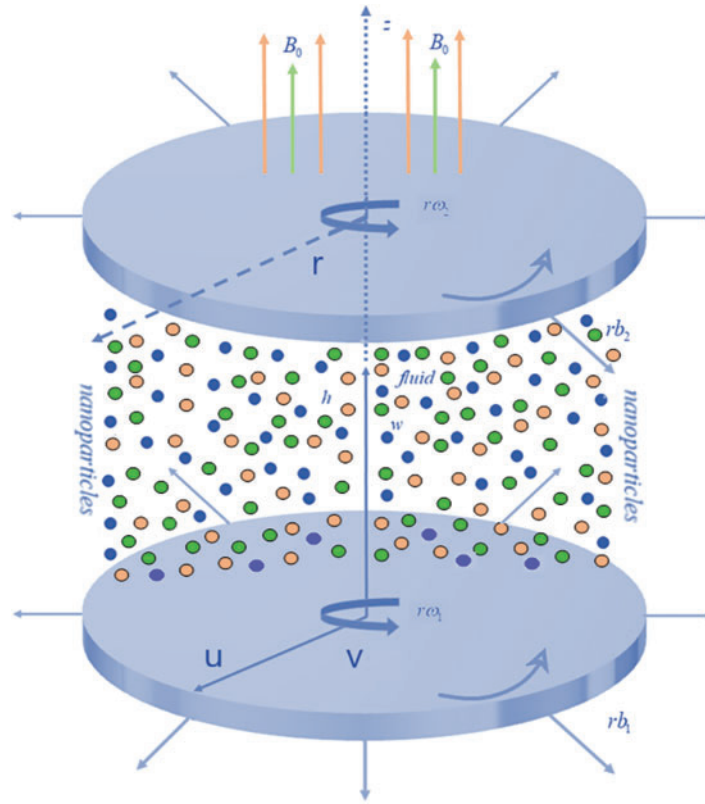


Figure 1: Physical configuration of flow issue

### 2.2 Dimensional Governing Boundary Flow Expressions

The governing flow equations are given bellow [36,37]:

$$\frac{\partial u}{\partial r} + \frac{u}{r} + \frac{\partial w}{\partial z} = 0, \tag{1}$$

$$\begin{aligned} & u \frac{\partial u}{\partial r} - \frac{v^2}{r} + w \frac{\partial u}{\partial z} + \lambda_1 \left( v^2 \frac{\partial^2 u}{\partial z^2} + u^2 \frac{\partial^2 u}{\partial r^2} + 2uv \frac{\partial^2 u}{\partial r \partial z} \right) \\ & = -\frac{1}{\rho_{nf}} \frac{\partial p}{\partial r} + \frac{\mu_{nf}}{\rho_{nf}} \left[ \frac{\partial^2 u}{\partial r^2} + \frac{\partial^2 u}{\partial z^2} + \frac{1}{r} \frac{\partial u}{\partial r} - \frac{u}{r^2} \right] - \frac{\nu_{nf}}{k^*} u + \frac{\sigma_{nf}}{\rho_{nf}} \beta_0^2 \left( -u - \lambda_1 v \frac{\partial u}{\partial z} \right), \end{aligned} \tag{2}$$

$$\begin{aligned} & u \frac{\partial v}{\partial r} + \frac{uv}{r} + w \frac{\partial v}{\partial z} + \lambda_1 \left( v^2 \frac{\partial^2 u}{\partial z^2} + u^2 \frac{\partial^2 u}{\partial r^2} + 2uv \frac{\partial^2 u}{\partial r \partial z} \right) \\ & = -\frac{1}{\rho_{nf}} \frac{\partial p}{\partial r} + \frac{\mu_{nf}}{\rho_{nf}} \left[ -\frac{v}{r^2} + \frac{\partial^2 v}{\partial r^2} + \frac{1}{r} \frac{\partial v}{\partial r} + \frac{\partial^2 v}{\partial z^2} \right] - \frac{\nu_{nf}}{k^*} v + \frac{\sigma_{nf}}{\rho_{nf}} \beta_0^2 \left( -v - \lambda_1 u \frac{\partial v}{\partial z} \right), \end{aligned} \tag{3}$$

$$u \frac{\partial w}{\partial r} + w \frac{\partial w}{\partial z} = -\frac{1}{\rho_{nf}} \frac{\partial p}{\partial z} + \frac{\mu_{nf}}{\rho_{nf}} \left[ \frac{1}{r} \frac{\partial w}{\partial r} + \frac{\partial^2 w}{\partial r^2} + \frac{\partial^2 w}{\partial z^2} \right], \tag{4}$$

$$\left( u \frac{\partial T}{\partial r} + w \frac{\partial T}{\partial z} \right) = \frac{k_{nf}}{(\rho c_p)_{nf}} \left[ \frac{\partial^2 T}{\partial r^2} + \frac{1}{r} \frac{\partial T}{\partial r} + \frac{\partial^2 T}{\partial z^2} \right] - \frac{1}{(\rho c_p)_{nf}} \frac{\partial q_r}{\partial z}, \tag{5}$$

With,

$$\begin{aligned} u &= rb_1, v = r\omega_1, w = 0, T = T_0, \text{ at } z = 0, \\ u &= rb_2, v = r\omega_2, w = 0, T = T_1, \text{ at } z = h. \end{aligned} \quad (6a)$$

The melting condition is addressed as

$$k_{nf} \left( \frac{\partial T}{\partial z} \right)_{z=0} = \rho_{nf} [L_0 + (c_p)_s (T_0 - T_1)] w. \quad (6b)$$

Here the electrical conductivity represented by  $\sigma_{nf}$ , the thermal diffusivity simplified as  $\alpha_{nf}$ , the density for nanofluid is  $\rho_{nf}$ ,  $T_0$  be the melting temperature, the nanofluid heat capacitance symbolized as  $(\rho c_p)_{nf}$ , the dynamic viscosity denoted by  $\mu_{nf}$ , the thermal conductivity for nanofluid demonstrated by  $k_{nf}$  the kinematic viscosity of base nanofluid characterized by  $\nu_f$ .

where  $nf$  elucidated the thermophysical properties of nanofluid, solid particles symbolized as  $s$ , base fluid can be written as  $f$  and the solid volume fraction denoted by  $\phi$  for fluid nanoparticles. "For the said flow the equation of continuity is satisfied for detail see Appendix".

Now by employing the Rosseland evaluation of radiative heat flux  $q_r$  is considered as

$$q_r = -\frac{4\sigma^*}{3K^*} \frac{\partial T^4}{\partial z} \quad (7)$$

Here consider that the heat transfers in the flow field are such that the expression  $T^4$  may be designed as thermal dependent linearly functions. This is capable by expending  $T^4$  in Taylor sequence about the ambient heat  $T_\infty$  as bellow described.

$$T^4 = T_\infty^4 + 4T_\infty^3(T - T_\infty) + 6T_\infty^2(T - T_\infty)^2 + \dots \quad (8)$$

In above Eq. (8) eliminate the terms of multi order and outer the first degree in  $(T - T_\infty)$  then we get:

$$T^4 \simeq 4T_\infty^3 T - 3T_\infty^4, \quad (9)$$

Now putting Eq. (9) into Eq. (7) then we have,

$$q_r = -\frac{16T_\infty^3 \sigma^*}{3K^*} \frac{\partial T}{\partial z}. \quad (10)$$

### 2.3 Similarity Transformations

The stream function  $\psi$  can be demarcated as follows [38]:

$$u = \frac{\partial \psi}{\partial y}, \quad v = -\frac{\partial \psi}{\partial x}. \quad (11)$$

The transformations are as follows:

$$\begin{aligned} u &= r\omega_1 f'(\zeta), \quad w = -2\omega_1 h f(\zeta), \quad v = r\omega_1 g(\zeta), \\ \zeta &= \frac{z}{h}, \quad \theta(\zeta) = \frac{T - T_1}{T_0 - T_1}, \quad p = \rho_f \omega_1 \nu_f \left( p(\zeta) + \frac{1}{2} \frac{r^2}{h^2} + \varepsilon \right). \end{aligned} \quad (12)$$

**2.4 Dimension-Less Equations**

After applying the similarity variables, we obtain the non-dimensional expressions are as follows:

$$f''' - \frac{A_1}{2} \text{Re}(-2ff''' + (f')^2 - g^2) - \text{Re}\beta A_1(f^2f''' - 2ff'f'') - A_2K\text{Re}f' - \frac{A_1}{A_2}M(f' + \beta ff'') - \frac{A_1}{A_2}\varepsilon = 0, \tag{13}$$

$$g'' + A_1\text{Re}(2fg' - 2f'g) - A_2K\text{Re}g - \frac{A_1}{A_2}M(g + \beta fg') = 0, \tag{14}$$

$$P' = 4A_2\text{Re}ff' + 2\frac{A_2}{A_1}f'', \tag{15}$$

$$(1 + Rd)\theta'' + 2\text{Re}PrA_3A_4f\theta' = 0, \tag{16}$$

With

$$\begin{aligned} \zeta = 0, \quad Pr\frac{\rho_f}{\rho_f}f(0) + Ma\frac{k_{nf}}{k_f}\theta'(0), \quad f' = B_1, \quad g = 1, \quad \theta' = 1, \\ \zeta = 1, \quad f' = B_2, \quad g = B_3, \quad \theta' = 0. \end{aligned} \tag{17}$$

**2.5 Non-Dimensional Parameters**

The dimension-less sundry parameters are given bellow:

$$\left[ \begin{aligned} \text{Re} = \frac{\omega_1 h^2}{\nu_f}, \quad Rd = \frac{16\sigma^* T_\infty^3}{3k_f K^*}, \quad M = \frac{\sigma\beta_0^2}{2\omega_1\rho_f}, \quad Pr = \frac{\nu_f}{\alpha_f}, \quad \beta = \lambda_1 a, \quad B_3 = \frac{\omega_1}{\omega_2}, \quad \left( B_1 = \frac{b_1}{\omega_1}, B_2 = \frac{b_2}{\omega_1} \right), \\ Ma = \frac{(c_p)_f(T_1 - T_1)}{L^* + (c_p)_s(T_0 - T_1)} \text{ and } A_1 = (1 - \phi)^{2.5} \left( 1 - \phi + \phi \left( \frac{\rho_s}{\rho_f} \right) \right), \quad A_2 = (1 - \phi) + \phi \left( \frac{\rho_s}{\rho_f} \right), \\ A_3 = (1 - \phi) + \phi \left( \frac{\rho C_p}_s \right), \quad A_4 = \frac{k_{nf}}{k_f}. \end{aligned} \right] \tag{18}$$

Here the Eq. (13) differentiated w.r.t. to  $\zeta$  and eliminate  $\varepsilon$  then we get shorter expression is as follows:

$$f^{iv} + A_1\text{Re}(ff'''' + gg') - A_2K\text{Re}f'' + \text{Re}\beta A_1(f^2f'''' + 2f'^2f'' + 2ff''^2) - \frac{A_1}{A_2}M(f'' + \beta f'f'' + \beta ff''') = 0. \tag{19}$$

Through Eqs. (13) and (17) the parameter  $\varepsilon$  which shows the pressure can be expressed as:

$$\begin{aligned} \varepsilon = \frac{A_2}{A_1}f''''(0) - A_2K\text{Re}f''(0) - \frac{A_2}{2}\text{Re}[(f'(0))^2 - 2f(0)f''(0) - g^2(0)] \\ - \text{Re}\beta A_2[(f(0))^2f''''(0) - 2f(0)f'(0)f''(0)] - M(f'(0) + \beta f'(0)f''(0)). \end{aligned} \tag{20}$$

The above Eq. (15) integrated with respect to  $\zeta$  and determined the pressure equation, by taking the limits starting (0 to  $\zeta$ ).

$$p + 2A_2\text{Re}f^2 + 2\frac{A_2}{A_1}(f' - f'(0)) = 0, \tag{21}$$

## 2.6 Physical Quantities

The Physical industrial inters in which the coefficients of skin frictions ( $C_1$  &  $C_2$ ) and the coefficients of Nusselt numbers ( $Nu_{x1}$  &  $Nu_{x2}$ ) for both discs are described.

$$C_1 = \frac{\tau_{rz}}{\rho_f(r\omega_1)^2}, C_2 = \frac{\tau_{\theta z}}{\rho_f(r\omega_2)^2}, \quad (22)$$

$$Nu_{x1} = \frac{hq_w}{k_f(T_0 - T_1)}, Nu_{x2} = \frac{hq_w}{k_f(T_0 - T_1)}. \quad (23)$$

Here we take stress ( $\tau_{zr}$  and  $\tau_{z\theta}$ ) elucidated the shear stresses for the lower disc along radial as well as tangential direction and the heat flux  $q_w$  correspondingly.

The skin frictions coefficients in non-dimensional forms are

$$C_1 = \frac{\tau_w|_{z=0}}{\rho_f(r\omega_1)^2} = \frac{1}{\text{Re}_r(1-\phi)^{2.5}} [(f''(0))^2 + (g'(0))^2]^{\frac{1}{2}}, \quad (24)$$

$$C_2 = \frac{\tau_w|_{z=h}}{\rho_f(r\omega_1)^2} = \frac{1}{\text{Re}_r(1-\phi)^{2.5}} [(f''(1))^2 + (g'(1))^2]^{\frac{1}{2}}, \quad (25)$$

And the coefficients of Nusselt numbers in non-dimensional forms are

$$Nu_1 = -(A_4 + Rd)\theta'(0), Nu_2 = -(A_4 + Rd)\theta'(1), \quad (26)$$

Here the total shear stress  $\tau_w$  addressed as:

$$\tau_w = \sqrt{\tau_{zr}^2 + \tau_{z\theta}^2} \quad (27)$$

## 3 Numerical Process: Finite Element Method (FEM)

Here, the nonlinear dimensionless ODE's (14)–(16) and (19) with specific boundary conditions (17) are tackled by utilizing the finite element method (FEM) or finite element analysis (FEA). These ODEs are highly nonlinear, so analytical techniques are not useful to solve these expressions. Therefore, the (FEM) is used to compute the solution of highly nonlinear system. The FEM is more effective than other technique.

### 3.1 Finite Element Technique (FET)

We get the exact solution through the finite element analysis the coupled nonlinearly ODE's structure (14)–(16) and (19) with specified boundary conditions (17) firstly we let

$$f' = s, f'' = s_1, f''' = s_2, f^{iv} = s_3, \quad (28)$$

$$s_3 + A_1 \text{Re}(f s_2 + g g') - A_2 K \text{Re} s_2 + \text{Re} \beta A_1 (f^2 s_2 + 2s^2 s_1 + 2f s_1^2) - \frac{A_1}{A_2} M (s_1 + \beta s s_1 + \beta f s_2) = 0, \quad (29)$$

$$g'' + A_1 \text{Re}(2f g' - 2f' g) - A_2 K \text{Re} g - \frac{A_1}{A_2} M (g + \beta f g') = 0, \quad (30)$$

$$P' - 4A_2 \text{Re} f s - 2 \frac{A_2}{A_1} s_1 = 0, \quad (31)$$

$$(1 + Rd)\theta'' + 2\text{Re Pr } A_3 A_4 f \theta' = 0. \tag{32}$$

With

$$\begin{aligned} \zeta = 0, \text{ Pr } \frac{\rho_{nf}}{\rho_f} f(0) + \text{Ma } \frac{k_{nf}}{k_f} \theta'(0), \quad s = B_1, \quad g = 1, \quad \theta' = 1, \\ \zeta = 1, \quad s = B_2, \quad g = B_3, \quad \theta' = 0. \end{aligned} \tag{33}$$

### 3.2 Variational Formulation

The variational method associated with the expressions (28)–(32) by typical linear component  $(\zeta_e, \zeta_{e+1})$  is explain as

$$\int_{\zeta_e}^{\zeta_{e+1}} \omega_1 \left( \frac{\partial f}{\partial \zeta} - s \right) d\zeta = 0, \tag{34}$$

$$\int_{\zeta_e}^{\zeta_{e+1}} \omega_2 \left[ s'' - \frac{A_1}{2} \text{Re}[s^2 - 2fs' - g^2] - A_2 K \text{Re}s' + -\text{Re}\beta A_1 [f^2 s'' - 2fss'] \right] d\zeta = 0, \tag{35}$$

$$\int_{\zeta_e}^{\zeta_{e+1}} \omega_3 \left[ g'' + A_1 \text{Re}[2fg' - 2hg] - A_2 K \text{Re}g - \frac{A_1}{A_2} M(g + \beta gg') \right] d\zeta = 0, \tag{36}$$

$$\int_{\zeta_e}^{\zeta_{e+1}} \omega_4 [(1 + Rd)\theta'' + 2A_3 A_4 \text{Pr } \text{Re}f \theta'] d\zeta = 0, \tag{37}$$

Here  $(\omega_1, \omega_2, \omega_3 \text{ and } \omega_4)$  described the arbitrary test functions and may be observed as the values in  $(f, s, g \text{ and } \theta)$  etc.

### 3.3 Finite-Element Description

Substitute finite element estimation of the form declared below; the finite element method may be attained from the abovementioned expressions:

$$f = \sum_{j=1}^3 f_j \psi_j, \quad s = \sum_{j=1}^3 s_j \psi_j, \quad g = \sum_{j=1}^3 g_j \psi_j, \quad \theta = \sum_{j=1}^3 \theta_j \psi_j, \tag{38}$$

By

$$\omega_1 = \omega_2 = \omega_3 = \omega_4 = \psi_i \quad (i = 1, 2, 3).$$

For typical components  $(\zeta_e, \zeta_{e+1})$ , the above-represented form function  $\psi_i$  can be defined as

$$\begin{aligned} \psi_1^e = \frac{(\zeta_{e+1} + \zeta_e - 2\zeta)(\zeta_{e+1} - \zeta)}{(\zeta_{e+1} - \zeta)^2}, \quad \psi_2^e = \frac{4(\zeta - \zeta_e)(\zeta_{e+1} - \zeta)}{(\zeta_{e+1} - \zeta)^2}, \\ \psi_3^e = \frac{(\zeta_{e+1} + \zeta_e - 2\zeta)(\zeta - \zeta_e)}{(\zeta_{e+1} - \zeta)^2}, \quad \zeta_e \leq \zeta \leq \zeta_{e+1}, \end{aligned} \tag{39}$$

The structure of finite-element method for nonlinear governing equations is mentioned as:

$$\begin{bmatrix} [K^{11}][K^{12}][K^{13}][K^{14}] \\ [K^{21}][K^{22}][K^{23}][K^{24}] \\ [K^{31}][K^{32}][K^{33}][K^{34}] \\ [K^{41}][K^{42}][K^{43}][K^{44}] \end{bmatrix} \begin{bmatrix} \{f\} \\ \{s\} \\ \{g\} \\ \{\theta\} \end{bmatrix} = \begin{bmatrix} \{r^1\} \\ \{r^2\} \\ \{r^3\} \\ \{r^4\} \end{bmatrix},$$

Here  $[K^{nm}]$  and  $[r^n]$  ( $m, n = 1, 2, 3, 4$ ) are established as

$$K_{ij}^{11} = \int_{\zeta_e}^{\zeta_{e+1}} \psi_i \frac{\partial \psi_j}{\partial \zeta} d\zeta, K_{ij}^{12} = - \int_{\zeta_e}^{\zeta_{e+1}} \psi_i \psi_j d\zeta, K_{ij}^{13} = 0, K_{ij}^{14} = 0,$$

$$K_{ij}^{21} = 0, K_{ij}^{23} = \frac{A_1}{2} \text{Re} \int_{\zeta_e}^{\zeta_{e+1}} \psi_i (\psi_j)^2 d\zeta, K_{ij}^{24} = 0,$$

$$K_{ij}^{22} = - \int_{\zeta_e}^{\zeta_{e+1}} \frac{\partial \psi_i}{\partial \zeta} \frac{\partial \psi_j}{\partial \zeta} d\zeta - \beta \text{Re} \left[ \int_{\zeta_e}^{\zeta_{e+1}} (\psi_i)^2 \frac{\partial \psi_i}{\partial \zeta} \frac{\partial \psi_j}{\partial \zeta} d\zeta + \int_{\zeta_e}^{\zeta_{e+1}} \psi_i \psi_j \frac{\partial \psi_j}{\partial \zeta} d\zeta \right]$$

$$+ \frac{A_1}{2} \text{Re} \bar{f}_1 \int_{\zeta_e}^{\zeta_{e+1}} \psi_i \psi_1 \frac{\partial \psi_j}{\partial \zeta} d\zeta + \frac{A_1}{2} \text{Re} \bar{f}_2 \int_{\zeta_e}^{\zeta_{e+1}} \psi_i \psi_2 \frac{\partial \psi_j}{\partial \zeta} d\zeta - K \text{Re} A_2 \int_{\zeta_e}^{\zeta_{e+1}} \psi_i \psi_j d\zeta$$

$$- \frac{A_1}{A_2} (M) \int_{\zeta_e}^{\zeta_{e+1}} \psi_i \psi_j d\zeta - \frac{A_1}{2} \text{Re} \int_{\zeta_e}^{\zeta_{e+1}} \psi_i (\psi_j)^2 d\zeta + \frac{A_1}{A_2} (M) \beta \bar{f}_1 \int_{\zeta_e}^{\zeta_{e+1}} \psi_i \psi_1 \frac{\partial \psi_j}{\partial \zeta} d\zeta$$

$$+ \frac{A_1}{A_2} M \beta \bar{f}_2 \int_{\zeta_e}^{\zeta_{e+1}} \psi_i \psi_2 \frac{\partial \psi_j}{\partial \zeta} d\zeta,$$

$$K_{ij}^{31} = 0, K_{ij}^{32} = -A_1 \text{Re} \bar{h}_1 \int_{\zeta_e}^{\zeta_{e+1}} \psi_i \psi_1 d\zeta + A_1 \text{Re} \bar{h}_2 \int_{\zeta_e}^{\zeta_{e+1}} \psi_i \psi_2 d\zeta, K_{ij}^{34} = 0,$$

$$K_{ij}^{33} = - \int_{\zeta_e}^{\zeta_{e+1}} \frac{\partial \psi_i}{\partial \zeta} \frac{\partial \psi_j}{\partial \zeta} d\zeta + A_1 \text{Re} \bar{f}_1 \int_{\zeta_e}^{\zeta_{e+1}} \psi_i \psi_1 \frac{\partial \psi_j}{\partial \zeta} d\zeta + A_1 \text{Re} \bar{f}_2 \int_{\zeta_e}^{\zeta_{e+1}} \psi_i \psi_2 \frac{\partial \psi_j}{\partial \zeta} d\zeta - \frac{A_1}{A_2}$$

$$K_{ij}^{41} = 0, K_{ij}^{42} = 0, K_{ij}^{43} = (1 + Rd) \int_{\zeta_e}^{\zeta_{e+1}} \frac{\partial \psi_i}{\partial \zeta} \frac{\partial \psi_j}{\partial \zeta} d\zeta + 2 \text{Pr} \text{Re} A_3 A_4 \bar{f}_1 \int_{\zeta_e}^{\zeta_{e+1}} \psi_i \psi_1 \frac{\partial \psi_j}{\partial \zeta} d\zeta$$

$$+ \frac{3}{4} A_3 A_4 \bar{f}_2 \int_{\zeta_e}^{\zeta_{e+1}} \psi_i \psi_2 \frac{\partial \psi_j}{\partial \zeta} d\zeta, K_{ij}^{44} = 0,$$

$$r_i^2 = 0, r_i^2 = - \left( \psi_i \frac{d\psi_i}{d\zeta} \right)_{\zeta_e}^{\zeta_{e+1}}, r_i^3 = - \left( \psi_i \frac{d\psi_i}{d\zeta} \right)_{\zeta_e}^{\zeta_{e+1}}, r_i^4 = - \left( \psi_i \frac{d\psi_i}{d\zeta} \right)_{\zeta_e}^{\zeta_{e+1}}.$$

### 3.4 Validation of Results

**Table 1:** Physical features [39] of particles and base liquid

Transport features	$\rho(kg/m^3)$	$C_p(J/kgK)$	$k(W/mK)$	$\sigma(Sm^{-1})$
Pure – $H_2O$	997.1	4179	0.613	0.05
Alumina( $Al_2O_3$ )	3970	765.0	40.000	$3.5 \times 10^7$
Titanium oxide $TiO_2$	4250	686.2	8.9538	$2.38 \times 10^6$

We used finite element method for tackling the nonlinear set of ODEs. Because fewer nodes are required in finite element, less memory is required to perform the full program, resulting in improved accuracy and, as a result, a shorter calculation time than FEM. Physical features like density, heat capacity, thermal conductivity and electrical conductivity of some particles and base liquid are given in Table 1. Characteristics for some physical properties of nanofluids are given in Table 2. For validation of code we compare current outcomes with the numerical outcomes found

by Lance et al. [40], Turkyilmazoglu [41] and Kumar et al. [42] for the rotation parameter  $B_3$  by fixed  $B_1 = B_2 = M = \phi = 0$  and  $Re = 1.0$  as summarized in Table 3. We observed good agreement between our results and published literature. Here minimal percentage errors are also display in Table 3.

**Table 2:** Characteristics of nanofluid

Properties	Nanofluid
dynamic Viscosity ( $\mu_{nf}$ )	$\mu_{nf} = \frac{\mu_f}{(1-\phi)^{2.5}}$ ,
Heat capacity $(\rho c_p)_{nf}$	$[\rho c_p]_{nf} = (1 - \phi)(\rho c_p)_f + (\rho c_p)_s \phi$ ,
Density ( $\rho_{nf}$ )	$\rho_{nf} = \rho_f(1 - \phi) + \rho_s \phi$ ,
Heat conductivity ( $k_{nf}$ )	$\frac{k_{nf}}{k_f} = \frac{(1-\phi)+2\phi \frac{k_s}{k_s-k_f} \ln\left(\frac{k_s+k_f}{2k_f}\right)}{(1-\phi)+2\phi \frac{k_f}{k_s-k_f} \ln\left(\frac{k_s+k_f}{2k_f}\right)}$ ,
Electrical conductivity ( $\sigma_{nf}$ )	$\sigma_{nf} = \left(1 + \frac{3\left(\frac{\sigma_s}{\sigma_f}-1\right)\phi}{\left(\frac{\sigma_s}{\sigma_f}+2\right)-\left(\frac{\sigma_s}{\sigma_f}-1\right)\phi}\right) \sigma_f$ ,
Thermal diffusivity ( $\alpha_{nf}$ )	$\alpha_{nf} = \frac{k_{nf}}{(\rho c_p)_{nf}}$ ,

**Table 3:** Validation of outcomes of distinguished amounts of  $B_3$  for  $f''(0)$  by selecting  $Re = 1.0$  when  $B_1 = B_2 = M = \phi = 0$

	Lance et al. [40]	Turkyilmazoglu [41]	Kumar et al. [42] (a)	Error percentage (b - a)/a $\times 100$	Current result (b)
$B_3$	$f''(0)$	$f''(0)$	$f''(0)$		$f''(0)$
-1.0	0.06666	0.06666313	0.06666320	0.000105005571	0.06666328
-0.8	0.08394	0.08394206	0.08394218	0.000142955748	0.08394232
-0.3	0.10395	0.10395088	0.10395114	0.000250118133	0.10395145
0.0	0.09997	0.09997221	0.09997268	0.000470130649	0.09997287
0.5	0.5 0.06663	0.06663419	0.06663447	0.000420204703	0.06663468

### 4 Results and Discussion

Fig. 2 indicates the radial velocity profile  $f'$  for varying variations in magnetic parameter  $M$  for  $Al_2O_3/water$  and  $TiO_2/water$  nanofluid flow between double radiative nanofluids. It is clearly illustrated that radial velocity field  $f'$  is reduced via magnetic parameter  $M$ . Magnetic parameter develops a resistance force known Lorentz force that is a delaying force in flow of fluid. The radial velocity component  $f'$  of Maxwell nanoliquid with change in Reynolds number  $Re$  is depicted in Fig. 3. From this picture it is learnt that the Reynolds number  $Re$  depresses the radial component of velocity  $f'$ . The physical reason for this is because when the lower disk rotates; the inertial impacts grow, slowing down the flow rate. Fig. 4 reveals the vital role of the radial velocity of fluid  $f'$  for the various variations of the nanoparticles volume fraction  $\phi$ . The increment in the velocity component  $f'$  is analyzed for higher nanoparticles volume fraction  $\phi$ . The converse relationship between the volume fraction and the dynamic viscosity of nanofluid causes the increase in velocity as a physical phenomenon. As a result, the viscosity of ordinary fluid is reduced in response to an increase in nanoparticle volume fraction, and fluid flow is increased [43]. The variation in radial velocity  $f'$  of water-based Maxwell single nanofluid with

stretching parameter  $B_2$  for upper disk is clarified in Fig. 5. It is mentioned that radial velocity  $f'$  of nanoliquid is depresses with stretching parameter for upper disk  $B_2$ . Fig. 6 illustrate the effect of fluid parameter  $\beta$  against radial flow  $f'$  of  $Al_2O_3/water$  and 44 nanofluid for distinguish values of fluid parameter  $\beta$ . Here we observed that larger fluid parameter  $\beta$ , decays the velocity of fluid. The radial velocity  $f'$  for  $Al_2O_3/water$  and  $TiO_2/water$  nanofluid against melting parameter  $Ma$  is elucidated in Fig. 7. Improve in melting parameter  $Ma$  reduces the radial velocity field  $f'$  of single nanoliquid inside parallel two disks. The significant decrement in radial velocity profile  $f'$  depicts in Fig. 8, due to growing variations of porosity parameter  $K$ . Fig. 9 is plotted to show the behavior of stretching parameter for upper disk  $B_2$  against tangential velocity  $g$  of  $Al_2O_3/water$  and  $TiO_2/water$  nanofluid flow. It is illustrated that with an increment in variation of stretching parameter  $B_2$ , the tangential flow  $g$  of nanofluid increases. Fig. 10 signifies the significant features of melting parameter  $Ma$  vs. tangential velocity  $g$  of  $Al_2O_3/water$  and  $TiO_2/water$  nanofluid flow over two parallel disks. It is examined that tangential velocity of fluid  $g$  is decreases via larger variations in the melting parameter  $Ma$ .

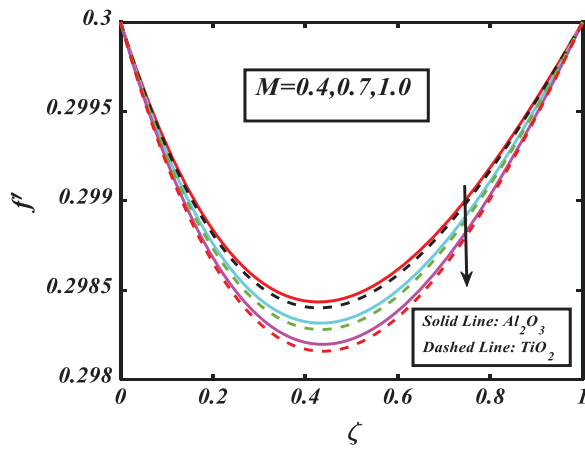


Figure 2: Importance of  $M$  via  $f'$

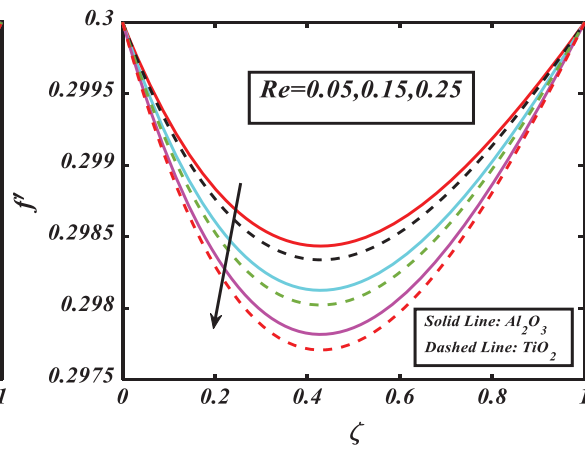


Figure 3: Importance of  $Re$  via  $f'$

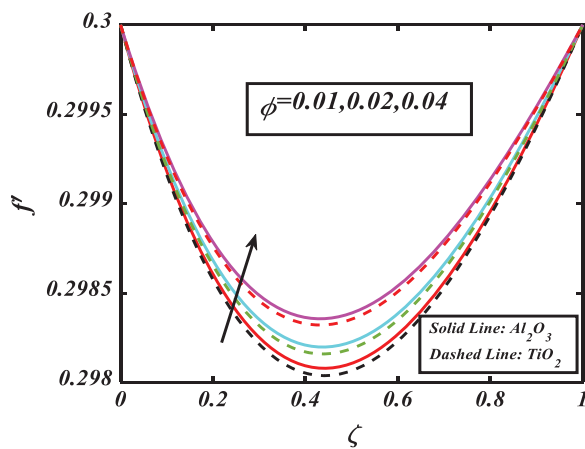


Figure 4: Importance of  $\phi$  via  $f'$

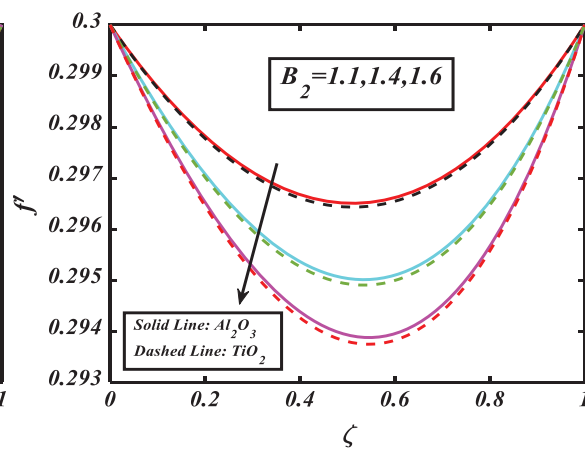
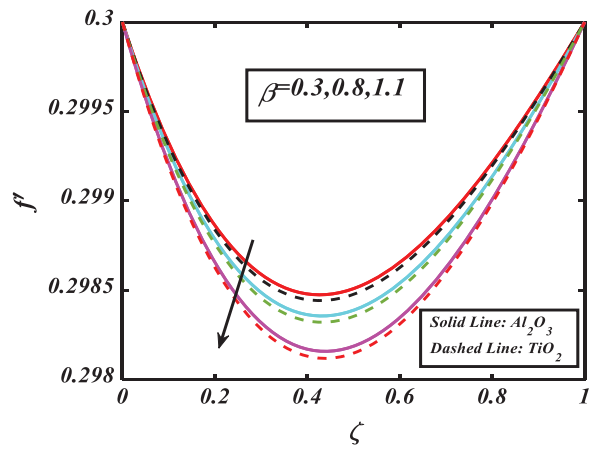
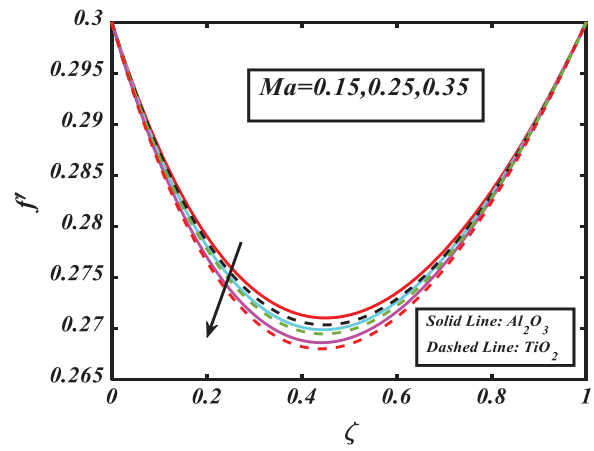


Figure 5: Importance of  $B_2$  via  $f'$



**Figure 6:** Importance of  $\beta$  via  $f'$



**Figure 7:** Importance of  $Ma$  via  $f'$

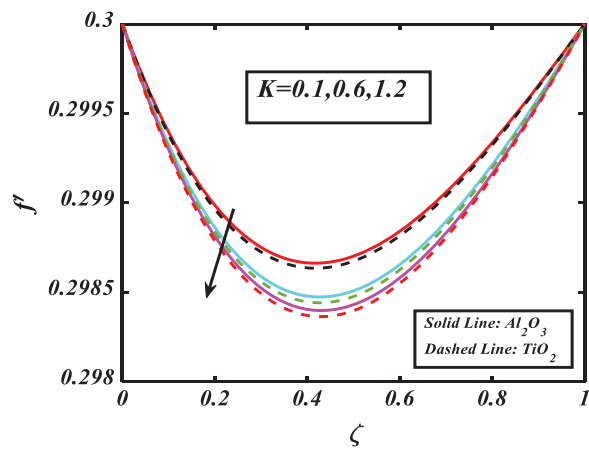


**Figure 8:** Importance of  $K$  via  $f'$

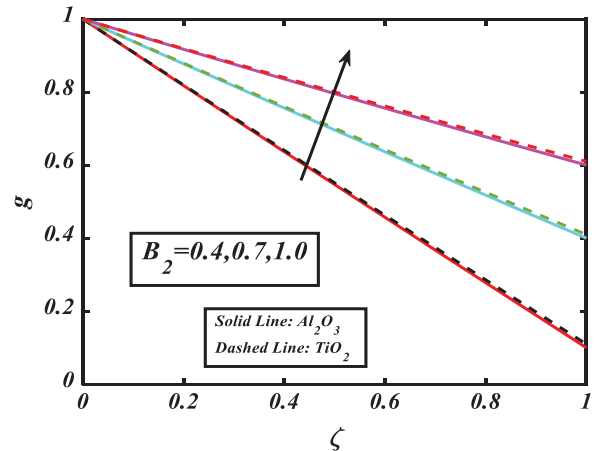


**Figure 9:** Importance of  $B_2$  via  $g$

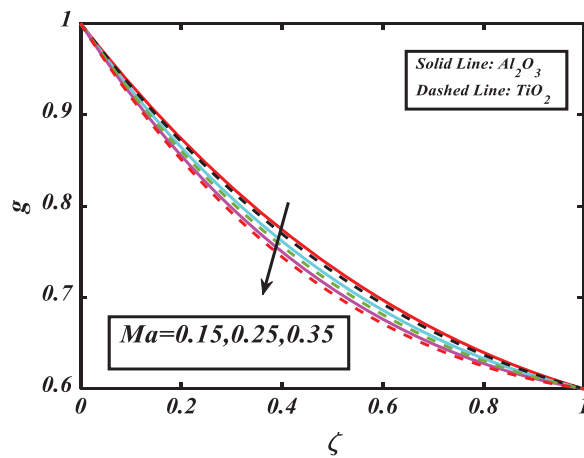


**Figure 10:** Importance of  $Ma$  via  $g$

The effect of thermal radiation parameter  $Rd$  against thermal field of nanomaterials  $\theta$  is disclosed in Fig. 11. It is analyzed that heat transfer  $\theta$  is increased with greater thermal radiation parameter  $Rd$ . Physically the absorption coefficient reduces for greater thermal radiation parameter and therefore the thermal field enhances. Fig. 12 examines the estimation in energy field  $\theta$  with different amounts of melting parameter  $Ma$  for  $Al_2O_3/water$  and  $TiO_2/water$  nanofluid flow over two parallel disks. We noted that temperature distribution  $\theta$  is decays via larger melting parameter  $Ma$ . Fig. 13 is designed to scrutinize the behavior of Prandtl number  $Pr$  against heat profile  $\theta$ . It is mentioned that by growing the Prandtl number  $Pr$ , the solutal field of species is declined. Since the Prandtl number indicates how quickly thermal diffusion occurs in compared to momentum diffusion, increasing the Prandtl number causes the thermal diffusivity to decrease and the temperature to drop. Fig. 14 shows that temperature distribution  $\theta$  is decreased with solid volume fraction  $\phi$  of  $Al_2O_3/water$  and  $TiO_2/water$  nanofluid flow.

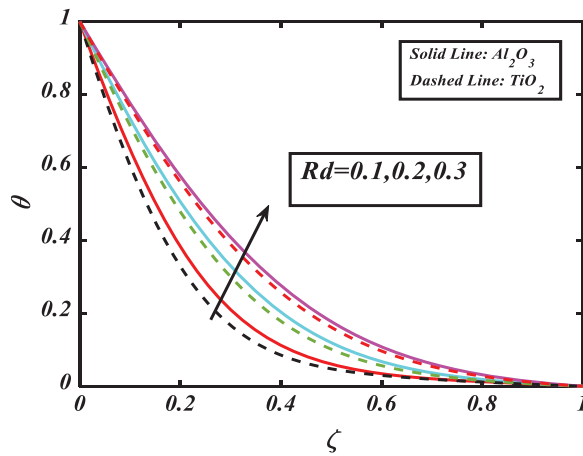


Figure 11: Importance of  $Rd$  via  $\theta$

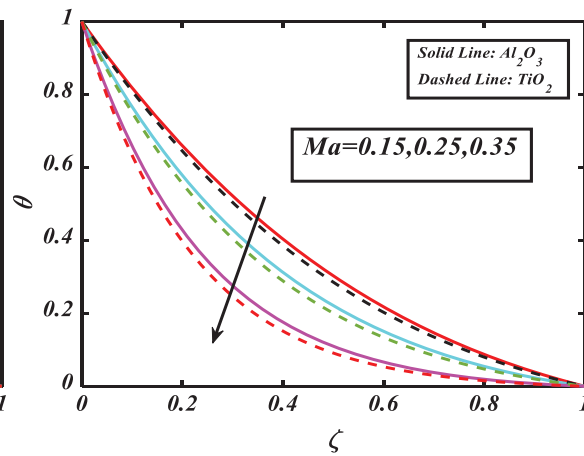


Figure 12: Importance of  $Ma$  via  $\theta$

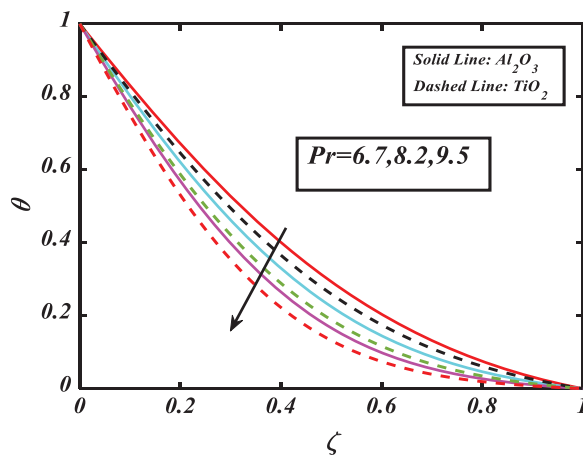


Figure 13: Importance of  $Pr$  via  $\theta$

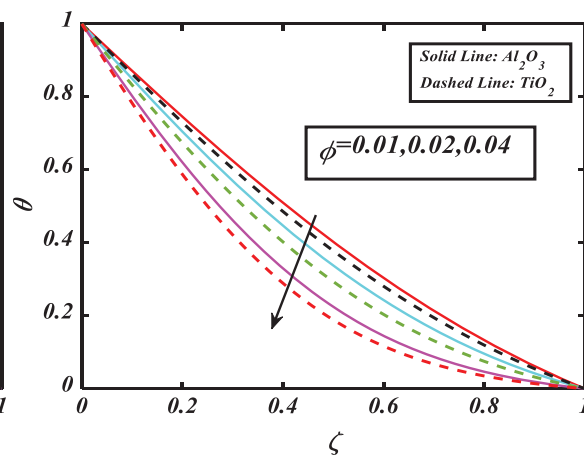


Figure 14: Importance of  $\phi$  via  $\theta$

## 5 Conclusions

The current study novelty is recent progress in melting heat transfer transportation of Maxwell  $Al_2O_3 - TiO_2/water$  nanofluid flow through double parallel rotating disks. The conclusive remarks of the present work are as follows:

- An increase in radial velocity of single Maxwell water-based nanofluid is analyzed vs. an improvement in nanoparticles volume friction.
- The radial velocity of nanofluid is reducing function of larger magnitudes of the melting parameter.
- The fluid flow declines with fluid parameter.
- The significant value of the tangential velocity is noticed via stretching parameter for upper disk.
- Temperature distribution raises for thermal radiation parameter.
- The thermal field of the fluid reduces as Prandtl number [44] increases.
- Larger solid volume friction decreases the temperature distribution.

**Acknowledgement:** This work was sponsored in part by National Natural Science Foundation of China (No. 51869031); and Science and Technology Research Program of Chongqing Municipal Education Commission (Grant No. KJQN201903801) and Huzhou Key Laboratory of Green Building Technology.

**Funding Statement:** This work is financially supported by the Government College University, Faisalabad and Higher Education Commission, Pakistan.

**Conflicts of Interest:** The authors declare that they have no conflicts of interest to report regarding the current analysis.

## References

1. Hayat, T., Khan, S. A., Khan, M. I., Alsaedi, A. (2019). Theoretical investigation of Ree–Eyring nanofluid flow with entropy optimization and arrhenius activation energy between two rotating disks. *Computer Methods and Programs in Biomedicine*, 177, 57–68. DOI 10.1016/j.cmpb.2019.05.012.
2. Qayyum, S., Khan, M. I., Hayat, T., Alsaedi, A., Tamoore, M. (2018). Entropy generation in dissipative flow of williamson fluid between two rotating disks. *International Journal of Heat and Mass Transfer*, 127, 933–942. DOI 10.1007/s11771-019-4082-y.
3. Muhammad, T., Waqas, H., Khan, S. A., Ellahi, R., Sait, S. M. (2021). Significance of nonlinear thermal radiation in 3D Eyring–Powell nanofluid flow with arrhenius activation energy. *Journal of Thermal Analysis and Calorimetry*, 143(2), 929–944. DOI 10.1007/s10973-020-09459-4.
4. Rafiq, T., Mustafa, M. (2020). Computational analysis of unsteady swirling flow around a decelerating rotating porous disk in nanofluid. *Arabian Journal for Science and Engineering*, 45(2), 1143–1154. DOI 10.1007/s13369-019-04257-z.
5. Hassan, M., Marin, M., Ellahi, R., Alamri, S. Z. (2018). Exploration of convective heat transfer and flow characteristics synthesis by Cu–Ag/water hybrid-nanofluids. *Heat Transfer Research*, 49(18), 1837–1848. DOI 10.1615/heattransres.2018025569.
6. Sheikholeslami, M., Ellahi, R. (2015). Electrohydrodynamic nanofluid hydrothermal treatment in an enclosure with sinusoidal upper wall. *Applied Sciences*, 5(3), 294–306. DOI 10.3390/app5030294.
7. Shah, Z., Sheikholeslami, M., Kumam, P. (2020). Influence of nanoparticles inclusion into water on convective magneto hydrodynamic flow with heat transfer and entropy generation through permeable domain. *Case Studies in Thermal Engineering*, 21, 100732. DOI 10.1016/j.csite.2020.100732.

8. Arefmanesh, A., Najafi, M., Nikfar, M. (2010). MLPG application of nanofluid flow mixed convection heat transfer in a wavy wall cavity. *Computer Modeling in Engineering & Sciences*, 69(2), 91–118. DOI 10.3970/cmcs.2010.069.091.
9. Ashraf, M. U., Qasim, M., Wakif, A., Afridi, M. I., Animasaun, I. L. (2020). A generalized differential quadrature algorithm for simulating magnetohydrodynamic peristaltic flow of blood-based nanofluid containing magnetite nanoparticles: A physiological application. *Numerical Methods for Partial Differential Equations*, 2020, 1–27. DOI 10.1002/num.22676.
10. Ullah, M. Z., Muhammad, T., Mallawi, F. (2021). On model for Darcy–Forchheimer 3D nanofluid flow subject to heat flux boundary condition. *Journal of Thermal Analysis and Calorimetry*, 143(3), 2411–2418. DOI 10.1007/s10973-020-09892-5.
11. Lu, L., Liu, L. H., Li, X. X. (2014). Investigation of squeezing unsteady nanofluid flow using the modified decomposition method. *Computer Modeling in Engineering & Sciences*, 101(1), 1–15. DOI 10.3970/cmcs.2014.101.001.
12. Li, Y. X., Muhammad, T., Bilal, M., Khan, M. A., Ahmadian, A. et al. (2021). Fractional simulation for darcy-forchheimer hybrid nanoliquid flow with partial slip over a spinning disk. *Alexandria Engineering Journal*, 60(5), 4787–4796. DOI 10.1016/j.aej.2021.03.062.
13. Gul, T., Bilal, M., Alghamdi, W., Asjad, M. I., Abdeljawad, T. (2021). Hybrid nanofluid flow within the conical gap between the cone and the surface of a rotating disk. *Scientific Reports*, 11(1), 1–19. DOI 10.1038/s41598-020-80750-y.
14. Waqas, H., Farooq, U., Naseem, R., Hussain, S., Alghamdi, M. (2021). Impact of MHD radiative flow of hybrid nanofluid over a rotating disk. *Case Studies in Thermal Engineering*, 26, 101015. DOI 10.1016/j.csite.2021.101015.
15. Shafee, A., Jafaryar, M., Alghamdi, M., Tlili, I. (2020). Entropy generation for spiral heat exchanger with considering NEPCM charging process using hybrid nanomaterial. *The European Physical Journal Plus*, 135(3), 1–15. DOI 10.1140/epjp/s13360-020-00284-0.
16. Armaghani, T., Sadeghi, M. S., Rashad, A. M., Mansour, M. A., Chamkha, A. J. et al. (2021). MHD mixed convection of localized heat source/sink in an  $\text{Al}_2\text{O}_3$ -cu/water hybrid nanofluid in L-shaped cavity. *Alexandria Engineering Journal*, 60(3), 2947–2962. DOI 10.1016/j.aej.2021.01.031.
17. Shoaib, M., Raja, M. A. Z., Sabir, M. T., Awais, M., Islam, S. et al. (2021). Numerical analysis of 3-D MHD hybrid nanofluid over a rotational disk in presence of thermal radiation with joule heating and viscous dissipation effects using lobatto IIIA technique. *Alexandria Engineering Journal*, 60(4), 3605–3619. DOI 10.1016/j.aej.2021.02.015.
18. Gul, T., Khan, A., Bilal, M., Alreshidi, N. A., Mukhtar, S. et al. (2020). Magnetic dipole impact on the hybrid nanofluid flow over an extending surface. *Scientific Reports*, 10(1), 1–13. DOI 10.1038/s41598-020-65298-1.
19. Waini, I., Ishak, A., Groşan, T., Pop, I. (2020). Mixed convection of a hybrid nanofluid flow along a vertical surface embedded in a porous medium. *International Communications in Heat and Mass Transfer*, 114, 104565. DOI 10.1016/j.icheatmasstransfer.2020.104565.
20. Ahmad, S., Nadeem, S., Khan, M. N. (2021). Enhanced transport properties and its theoretical analysis in two-phase hybrid nanofluid. *Applied Nanoscience*, 2021, 1–8. DOI 10.1007/s13204-020-01634-1.
21. Reddy, P. S., Sreedevi, P., Chamkha, A. J. (2017). MHD boundary layer flow, heat and mass transfer analysis over a rotating disk through porous medium saturated by Cu-water and Ag-water nanofluid with chemical reaction. *Powder Technology*, 307, 46–55. DOI 10.1016/j.powtec.2016.11.017.
22. Wakif, A., Boulaia, Z., Ali, F., Eid, M. R., Sehaqui, R. (2018). Numerical analysis of the unsteady natural convection MHD couette nanofluid flow in the presence of thermal radiation using single and two-phase nanofluid models for Cu–water nanofluids. *International Journal of Applied and Computational Mathematics*, 4(3), 1–27. DOI 10.1007/S40819-018-0513-Y.
23. Mumraiz, S., Ali, A., Awais, M., Shutaywi, M., Shah, Z. (2021). Entropy generation in electrical magnetohydrodynamic flow of  $\text{Al}_2\text{O}_3$ -Cu/ $\text{H}_2\text{O}$  hybrid nanofluid with non-uniform heat flux. *Journal of Thermal Analysis and Calorimetry*, 143(3), 2135–2148. DOI 10.1007/s10973-020-09603-0.

24. Sheikholeslami, M. (2018). Cu-water nanofluid flow due to magnetic field inside a porous media considering brownian motion. *Journal of Molecular Liquids*, 249, 921–929. DOI 10.1016/j.molliq.2017.11.118.
25. Waqas, H., Shehzad, S. A., Khan, S. U., Imran, M. (2019). Novel numerical computations on flow of nanoparticles in porous rotating disk with multiple slip effects and microorganisms. *Journal of Nanofluids*, 8(7), 1423–1432. DOI 10.1166/jon.2019.1702.
26. Riaz, A., Khan, S. U. D., Zeeshan, A., Khan, S. U., Hassan, M. et al. (2021). Thermal analysis of peristaltic flow of nanosized particles within a curved channel with second-order partial slip and porous medium. *Journal of Thermal Analysis and Calorimetry*, 143(3), 1997–2009. DOI 10.1007/s10973-020-09454-9.
27. Hayat, T., Ijaz, M., Farooq, M., Alsaedi, A., Yasmeen, T. (2017). Impact of marangoni convection in the flow of carbon–water nanofluid with thermal radiation. *International Journal of Heat and Mass Transfer*, 106, 810–815. DOI 10.1016/j.ijheatmasstransfer.2016.08.115.
28. Sheikholeslami, M., Shamlooei, M. (2017).  $\text{Fe}_3\text{O}_4\text{-H}_2\text{O}$  nanofluid natural convection in presence of thermal radiation. *International Journal of Hydrogen Energy*, 42(9), 5708–5718. DOI 10.1016/j.ijhydene.2017.02.031.
29. Li, Y., Hassan, W., Muhammad, I., Umar, F., Fouad, M. et al. (2020). A numerical exploration of modified second-grade nanofluid with motile microorganisms, thermal radiation, and Wu's slip. *Symmetry*, 12(3), 393. DOI 10.3390/sym12030393.
30. Naqvi, S. M. R. S., Muhammad, T., Asma, M. (2020). Hydromagnetic flow of casson nanofluid over a porous stretching cylinder with newtonian heat and mass conditions. *Physica A: Statistical Mechanics and its Applications*, 550, 123988. DOI 10.1016/j.physa.2019.123988.
31. Roberts, L. (1958). On the melting of a semi-infinite body of ice placed in a hot stream of air. *Journal of Fluid Mechanics*, 4(5), 505–528. DOI 10.1017/S002211205800063X.
32. Waqas, H., Khan, S. A., Farooq, U., Khan, I., Alotaibi, H. et al. (2021). Melting phenomenon of non-linear radiative generalized second grade nanoliquid. *Case Studies in Thermal Engineering*, 26, 101011. DOI 10.1016/j.csite.2021.101011.
33. Hayat, T., Shah, F., Alsaedi, A., Waqas, M. (2018). Numerical simulation for magneto nanofluid flow through a porous space with melting heat transfer. *Microgravity Science and Technology*, 30(3), 265–275. DOI 10.1007/s12217-018-9595-8.
34. Ullah, I., Hayat, T., Alsaedi, A., Fardoun, H. M. (2021). Numerical treatment of melting heat transfer and entropy generation in stagnation point flow of hybrid nanomaterials (SWCNT-mWCNT/engine oil). *Modern Physics Letters B*, 35(6), 2150102. DOI 10.1142/S0217984921501025.
35. Sharma, R. P., Acharya, N., Das, K. (2020). On the impact of variable thickness and melting transfer of heat on magnetohydrodynamics nanofluid flow past a slandering stretching sheet. *Indian Journal of Geo-Marine Sciences*, 49(4), 641–648.
36. Jyothi, K., Reddy, P. S., Reddy, M. S. (2018). Influence of magnetic field and thermal radiation on convective flow of SWCNTs-water and MWCNTs-water nanofluid between rotating stretchable disks with convective boundary conditions. *Powder Technology*, 331, 326–337. DOI 10.1016/j.powtec.2018.03.020.
37. Reddy, P. S., Jyothi, K., Reddy, M. S. (2018). Flow and heat transfer analysis of carbon nanotubes-based Maxwell nanofluid flow driven by rotating stretchable disks with thermal radiation. *Journal of the Brazilian Society of Mechanical Sciences and Engineering*, 40(12), 1–16. DOI 10.1007/s40430-018-1494-9.
38. Khan, M., Rasheed, A. (2021). Slip velocity and temperature jump effects on molybdenum disulfide  $\text{MoS}_2$  and silicon oxide  $\text{SiO}_2$  hybrid nanofluid near irregular 3D surface. *Alexandria Engineering Journal*, 60(1), 1689–1701. DOI 10.1016/j.aej.2020.11.019.
39. Ahmed, J., Shahzad, A., Farooq, A., Kamran, M., Khan, S. U. D. et al. (2021). Thermal analysis in swirling flow of titanium dioxide–aluminum oxide water hybrid nanofluid over a rotating cylinder. *Journal of Thermal Analysis and Calorimetry*, 144(6), 2175–2185. DOI 10.1007/s10973-020-10190-3.
40. Lance, G. N., Rogers, M. H. (1962). The axially symmetric flow of a viscous fluid between two infinite rotating disks. *Proceedings of the Royal Society of London. Series A. Mathematical and Physical Sciences*, 266(1324), 109–121. DOI 10.1098/rspa.1962.0050.

41. Turkyilmazoglu, M. (2016). Flow and heat simultaneously induced by two stretchable rotating disks. *Physics of Fluids*, 28(4), 043601. DOI 10.1063/1.4945651.
42. Kumar, R., Seth, G. S., Bhattacharyya, A. (2019). Entropy generation of von karman's radiative flow with  $Al_2O_3$  and Cu nanoparticles between two coaxial rotating disks: A finite-element analysis. *The European Physical Journal Plus*, 134(12), 1–20. DOI 10.1140/epjp/i2019-13086-0.
43. Ahmad, F., Waqas, H., Ayed, H., Hussain, S., Farooq, S. et al. (2021). Numerical treatment with lobatto-iiia scheme magneto-thermo-natural convection flow of casson nanofluid ( $MoS_2-Cu/SA$ ) configured by a stretching cylinder in porous medium with multiple slips. *Case Studies in Thermal Engineering*, 26, 101132. DOI 10.1016/j.csite.2021.101132.
44. Sreedevi, P., Reddy, P. S., Sheremet, M. (2020). A comparative study of  $Al_2O_3$  and  $TiO_2$  nanofluid flow over a wedge with non-linear thermal radiation. *International Journal of Numerical Methods for Heat & Fluid Flow*, 30(3), 1291–1317. DOI 10.1108/HFF-05-2019-0434.

## Appendix

$$\frac{\partial u}{\partial r} + \frac{u}{r} + \frac{\partial w}{\partial z} = 0, \quad (A1)$$

We have

$$\begin{aligned} \frac{\partial u}{\partial r} &= r\omega_1 f', \\ \frac{\partial u}{\partial z} &= -2\omega_1 f', \end{aligned}$$

and

$$\frac{u}{r} = \omega_1 f'$$

Putting all required values in Eq. (A1) we, have

$$= r\omega_1 f' + \omega_1 f' - 2\omega_1 f' = 0$$

Hence equation of continuity trivially satisfied.